

# Vehicle Body Vibration and Noise Impact on Driver and Passengers Analysis: The Case of the 29-Seat Thaco Garden TB79s Bus

**Vu Hai Quan**

School of Mechanical and Automotive Engineering, Hanoi University of Industry, Hanoi, Vietnam  
quanvh@hau.edu.vn (corresponding author)

**Duong Quang Uy**

School of Mechanical and Automotive Engineering, Hanoi University of Industry, Hanoi, Vietnam  
duongquanguy03@gmail.com

Received: 8 October 2024 | Revised: 5 November 2024 and 26 November 2024 | Accepted: 12 December 2024

Licensed under a CC-BY 4.0 license | Copyright (c) by the authors | DOI: <https://doi.org/10.48084/etasr.9200>

## ABSTRACT

Noise, Vibration, and Harshness (NVH) are critical factors influencing the comfort and satisfaction of vehicle occupants. NVH encompasses the sound levels generated during vehicle operation, the vibrations transmitted through the vehicle structure, and the perceived harshness of the ride quality. This study focuses on the NVH analysis of the Thaco Garden TB79s, a 29-seat passenger vehicle. The Finite Element Method (FEM) is applied to simulate the impact on the vehicle as it traverses two types of road surfaces, characteristic of Vietnam: rumble strips with varying frequencies and uneven roads with random excitation. The results reveal that the Sound Pressure Level (SPL) is within the frequency range from 0 to 200 Hz while the vehicle navigates on rumble strips. Further analysis of the vehicle's body and the air mass within the cabin identifies a resonance phenomenon at the driver's ear location at 176 Hz, resulting in a maximum SPL of 166.92 dB. Additionally, the study examines the noise formation within the cabin during a 25-second period as the vehicle travels over random road surfaces. The maximum sound pressure at the driver's position reaches 0.24 psi, with the SPL fluctuating primarily between 130 and 155 dB.

*Keywords-NVH; natural vibration; finite element method*

## I. INTRODUCTION

NVH plays a critical role in the comfort and well-being of vehicle occupants. However, excessive NVH can cause discomfort, fatigue, and reduced concentration, making its management particularly important for passenger vehicles. Consequently, automotive manufacturers increasingly prioritize NVH optimization. To address this issue, local experts employ a variety of methods, such as experimental analysis and simulation, to assess and mitigate vehicle vibration and noise. Specifically, authors in [1] evaluated the aerodynamic noise on passenger car bodies using the Computational Fluid Dynamics (CFD) method along with the ANSYS Fluent R16 software. Similarly, authors in [2] analyzed the impact of the internal combustion engine vibration on driving comfort, while authors in [3] utilized the Comsol Multiphysics software to simulate differential vibration and noise. Authors in [4] investigated the vibration response of car body structures under engine excitation. Furthermore, the work in [5] involved generating random road surface profiles using MATLAB software based on the international standard ISO 8608. These profiles were then applied to evaluate the motion comfort effect for passengers traveling in sleeper coaches.

Globally, NHV research remains a vital area of focus, with numerous being annually studies published. Authors in [6] addressed the issue of vehicle noise employing Active Noise Control (ANC), achieving an average noise reduction of 3.4 dB at the driver's seat and the rear right seat at a frequency of 400 Hz. Authors in [7] investigated the noise levels in 13 passenger vehicles, indicating that the internal combustion engine compartment exhibited the highest noise levels, exceeding 90 dB, with increases being observed over prolonged use. Additionally, authors in [8] demonstrated that the Active Structural Acoustic Control (ASAC) systems installed on windshields could reduce the SPL by up to 15 dB. Similarly, authors in [9] analyzed cabin acoustics using a simplified model that excluded chassis and suspension components. In [10], a truck frame model was utilized to investigate natural frequencies and mode shapes, bypassing the tires and suspension system to assess the vibrations from the engine and road surface. Such equivalent models are commonly used in NVH analysis [11-15].

The object of this study was a common type of passenger car, manufactured and assembled in Vietnam. The boundary conditions for determining the excitation factors causing vibration were established according to the standard TCCS

34:2020/TCDBVN [16]. The research study focused on examining the effect of the sound pressure values on the drivers and passengers within the vehicle. Simulations were conducted at multiple locations, evenly distributed throughout the vehicle's interior space. The results were compared with medical standards to provide actionable recommendations for vehicle operation and design.

## II. THEORY BACKGROUND

### A. Sound Pressure

Sound pressure (Pa), or negative pressure, represents the local deviation in the atmospheric pressure caused by a sound wave. In air, it can be measured using a microphone, and in water, with a hydrophone.

### B. Sound Pressure Level (SPL)

The SPL quantifies a sound intensity relative to a fixed reference level (dB). It measures the strength of the sound perceived by the human ear. The SPL is defined as:

$$SPL = 10 \log_{10} \left[ \frac{p_{rms}^2}{p_{ref}^2} \right] = 20 \log_{10} \left[ \frac{p_{rms}}{p_{ref}} \right] \quad (1)$$

where  $SPL$  is the SPL,  $p_{ref}$  is the reference pressure level equal to 20  $\mu$ Pa, and  $p_{rms}$  is the root-mean-square sound pressure:

$$p_{rms} = \frac{p_{max}^2}{2} \quad (2)$$

with  $p_{max}$  being the maximum sound pressure.

### C. Fourier Transform

The Fourier transform decomposes a signal into its frequency components, allowing for the analysis of its frequency structure. It converts a signal from the time domain to the frequency domain, using:

$$X(f) = \int_{-\infty}^{\infty} x(t) e^{-j2\pi ft} dt \quad (3)$$

where  $X(f)$  is the amplitude of the signal at a  $f$  frequency, and  $x(t)$  is the signal in the time domain.

### D. Normal Modes Analysis

The natural frequencies of a system are determined by the structure's rigidity, mass, and boundary conditions. For a vehicle shell structure, the governing equation of motion is:

$$M\ddot{x} + C\dot{x} + Kx = f(t) \quad (4)$$

where  $M$  is the mass matrix of the structure,  $K$  is the stiffness matrix of the structure,  $C$  is the damping matrix,  $\ddot{x}$  is the acceleration vector,  $\dot{x}$  is the velocity vector,  $x$  is the displacement vector, and  $f(t)$  is the time-varying load vector.

Ignoring the external forces and the damping effects, (4) is simplified to:

$$M\ddot{x} + Kx = 0 \quad (5)$$

This describes the free vibration. Assuming a solution of the form:

$$x = \phi \sin(\omega t) \quad (6)$$

we arrive at the eigenvalue problem:

$$\begin{aligned} -\omega^2 M \phi \sin(\omega t) + K \phi \sin(\omega t) &= 0 \\ (K - \omega^2 M) \phi &= 0 \end{aligned} \quad (7)$$

where  $\phi$  is the mode shape vector and  $\omega$  the natural frequency. The solution of the eigenvalue problem yields  $n$  eigenvalues  $\lambda$ , where  $n$  is the number of the degrees-of-freedom. Vector  $\phi$  is the eigenvector corresponding to the eigenvalue.

### E. Model Frequency Response Analysis

The model analysis involves solving the eigenvalue problem to obtain eigenvalues  $\lambda_i$  and eigenvectors  $A$ . Assuming a displacement solution:

$$u = A d e^{i\Omega t} \quad (8)$$

the equation of motion is then transformed into modal coordinates using the eigenvectors:

$$[-\Omega A^T M A + A^T K A] d e^{i\Omega t} = A^T f e^{i\Omega t} \quad (9)$$

where  $A^T M A$  and  $A^T K A$  are the mass and stiffness matrices respectively, which are diagonal.

Applying the damping values introduces:

$$[-\Omega^2 m_i + i\Omega C_i + k_i] d e^{i\Omega t} = f_i e^{i\Omega t} \quad (10)$$

where:  $\zeta_i = \frac{c_i}{2m_i\omega_i}$  is the model damping ratio and  $\omega_i^2$  is the model eigenvalue.

Three types of damping values  $g_i$  ( $f_i^{freq}$ ) can be defined:

$$G = \zeta_i = \frac{c_i}{c_{cr}} = \frac{g_i}{2} \quad (11)$$

$$CRIT = C_{Cr} = 2m_i\omega_i \quad (12)$$

$$Q = Q_i = \frac{1}{2\zeta_i} = \frac{1}{g_i} \quad (13)$$

where  $G$  is the structural damping,  $CRIT$  is the critical damping, and  $Q$  is the quality factor.

Modal damping is entered into the complex stiffness matrix as structural damping if  $PARAM, KDAMP, -1$  is used. Then the uncoupled equation becomes:

$$[-\Omega^2 m_i + (1 + ig(\Omega))k_i] d e^{i\Omega t} = f_i e^{i\Omega t} \quad (14)$$

### F. Model Transient Response Analysis

The transient response calculates the structural reactions solving the equation of motion with the initial conditions being in the form of a matrix:

$$M\ddot{u} + B\dot{u} + ku = f(t) \quad (15)$$

$$\begin{cases} u(t=0) = u_0 \\ \dot{u}(t=0) = \dot{u}_0 \\ \ddot{u}(t=0) = \ddot{u}_0 \end{cases} \quad (16)$$

where  $f(t)$  is the time dependent load,  $M$  is the mass matrix,  $B$  is the damping matrix,  $K$  is the stiffness matrix,  $\ddot{u}, \dot{u}, u$  are the acceleration, velocity, and displacement time dependents, and  $\ddot{u}_0, \dot{u}_0, u_0$  are the initial conditions of the problem.

An analysis of conventional methods obtains eigenvalues and their corresponding eigenvectors. The u-state vector  $\lambda_i = \omega_i^2 A = A_i$  can be represented as the scalar product of eigenvectors  $A$  and the modal reaction  $v$ :

$$u = Av \tag{17}$$

The equation of motion without damping is then converted into modal coordinates using separate vectors:

$$A^T MA\ddot{v} + A^T kAv = A^T f \tag{18}$$

This way the system equation is reduced to a set of uncoupled equations for the components of  $v$  that can be easily solved. The inclusion of damping yields:

$$A^T MA\ddot{v} + A^T CA\dot{v} + A^T kAv = A^T f \tag{19}$$

where  $A^T CA$  is a non-diagonal matrix.

The separation of equations can be maintained if the damping factor is applied to each equation separately.

### III. RESULTS AND DISCUSSION

The simulation problem was conducted using two types of profiles that were characterized and defined according to the standard TCCS 34:2020/TCDBVN [16]. The design simulation model was based on a typical passenger car, with actual vehicle dimensions used for accuracy. For simplicity, assumptions were made to exclude the suspension system and other sources of noise within the vehicle. The evaluation focused on the simulation results at four node point locations.

#### A. Finite Element Model

This study employs the FEM to model the Thaco Garden TB79s body shell, displayed in Figure 1(a). The FEM model is combined with an acoustic model, observed in Figure 1(b), to investigate the interior cabin noise and assess the impact of the vibration-induced noise on humans, with particular attention being paid to the driver's position.

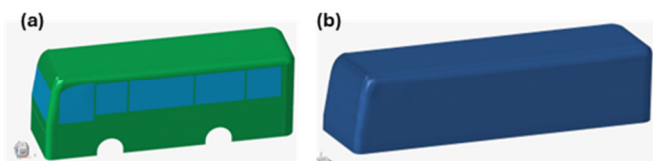


Fig. 1. (a) FEM model of car body shells, (b) FEM model and acoustic model of cabin.

When the vehicle is in motion, the road forces are transmitted to the frame through the suspension system. However, due to limitations in equipment and technology, this study focuses exclusively on the vibrations transmitted through the vehicle body and their impact on the passengers, excluding other noise-generating systems.

#### B. Normal Mode Analysis in Car Body Shells

Table I presents the input material parameters of the different parts of the vehicle. In some NHV analyses, the sound pressure is calculated after being simulated by the motor at approximately 50 Hz [17], or by the pavement with typical values ranging from 0 to 100 Hz [18]. For this study, a

simulation from poor terrain road surfaces with a frequency ranging from 0 to 200 Hz was selected. The frequency values will be obtained within this range throughout the simulation process. Table II depicts a sample of the natural frequencies including the first six types of natural vibration. Figure 2 illustrates the natural vibrations of the vehicle body at frequencies of 1.72 Hz and 176.44 Hz.

TABLE I. INPUT MATERIAL PARAMETERS

Part	Floor	Car body shells	Windshield	Window
Material	Steel	Steel	Glass	Glass
Young's Modulus (GPa)	210000		70000	
Poisson's ratio	0.3		0.3	
Density (kg/m <sup>3</sup> )	7850		2700	
Thickness (mm)	1.5	0.7	7	5

TABLE II. NATURAL FREQUENCIES OF THE FIRST 6 TYPES OF NATURAL VIBRATION

Natural vibration	Natural frequency (Hz)
1	1.01
2	1.02
3	1.05
4	1.11
5	1.14
6	1.15

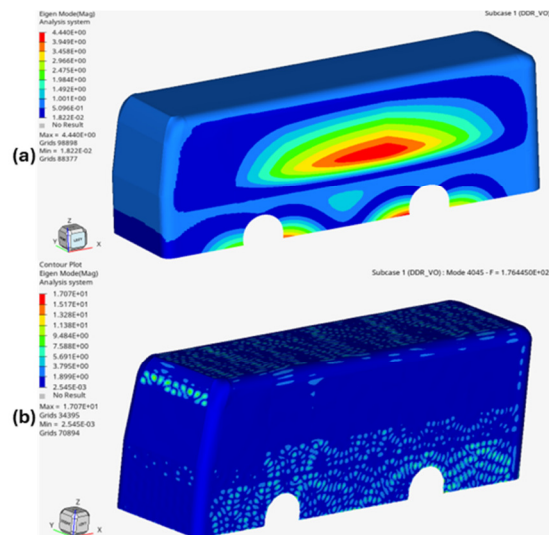


Fig. 2. Natural vibration of car body shells in modes (a) 16 ( $f = 1.72$  Hz) and (b) 4045 ( $f = 176.44$  Hz).

At lower frequencies, the entire vehicle body tends to vibrate as a single mass, with all surface points participating in the motion. This results in large vibration zones with a relatively uniform distribution of the vibrational energy, making high-amplitude vibrations visible across extensive regions. At higher frequencies, the vehicle body exhibits multiple natural vibration modes. Each mode has a distinct shape, with the motion being concentrated at specific points on the surface. The appearance of numerous small vibration points indicates that the vibrational energy is no longer evenly distributed but is instead focused on particular locations. The results demonstrate that the natural frequencies of the vehicle body fall within the 200 Hz range. Each vibration mode

responds uniquely, enabling predictions of the system’s behavior when external forces are applied at its natural frequencies.

C. Natural Mode Analysis in Cabin Acoustic Model

An acoustic model is being employed to analyze the natural vibrations of the cabin acoustic model. Table III illustrates the initial parameters of the cabin acoustic model.

TABLE III. INPUT PARAMETERS OF THE CABN ACOUSTIC MODEL

Material	Density (kg/m <sup>3</sup> )	Speed of sound (m/s)
air	1125	340

The natural frequency range of the cabin acoustic model is established using the same method as the analysis of the natural vibration of the car body shells. Table IV presents a sample of the natural vibration and its frequencies.

TABLE IV. NATURAL FREQUENCIES OF THE ACOUSTIC MODEL

Natural vibration	Natural frequency (Hz)
1	1.38e-5
2	20.68
3	41.36
4	61.98
...	...
42	176.46
...	...
59	199.94

In the frequency range of 0 to 200 Hz, 59 vibration modes of the air mass were identified. Each mode highlights specific localized areas within the cabin where sound pressure reaches its maximum, indicating points of heightened acoustic intensity. Additionally, these modes also demonstrate the interaction between the sound pressure and the surrounding air mass, illustrating how pressure fluctuations propagate throughout the cabin environment. Each identified vibration mode exhibits a unique air pressure distribution. This variation in pressure distribution plays a crucial role in influencing the propagation and resonance of the sound waves within the cabin, ultimately shaping the overall acoustic experience for the passengers.

Figure 3 displays two natural vibrations of the cabin acoustic model at frequencies of 20.68 Hz and 176.46 Hz. At the higher natural frequency, the system exhibits multiple complex vibrational modes. These modes create small, unevenly distributed vibration regions, as energy becomes concentrated at specific points. This phenomenon arises due to the presence of numerous nodal points and antinodes, leading to intricate vibration patterns characterized by a non-uniform energy distribution. In contrast, at the lower natural frequency, the system behaves more like a homogeneous mass vibrating as a single entity. The energy is distributed more evenly across larger areas, resulting in broader vibration zones. For instance, large vibration areas, such as the entire front section of the vehicle, are clearly observable.

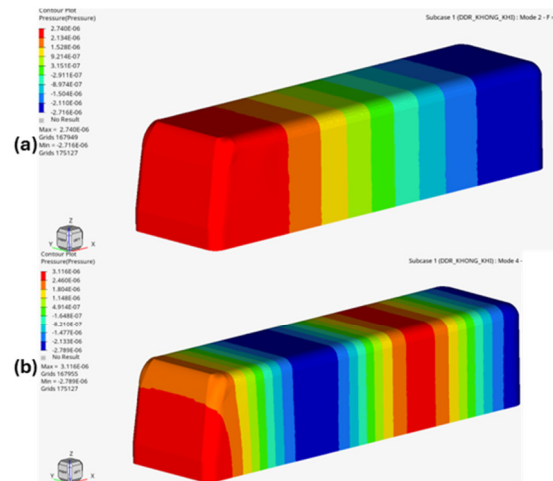


Fig. 3. Natural vibration of cabin acoustic model in modes (a) 2 (f=20.68 Hz) and (b) 4 (f = 176.46 Hz)

D. Noise Analysis Problem at the Driver’s Position after the Car Moves on the "Rumble Strips" Speed Bump

This analysis examines the SPL at the driver’s position as the vehicle moves over rumble strip speed bumps. The amplitude of the excitation force is held constant during the frequency surveys. The aggregated SPL reflects variations across all frequencies, simulating the effects of a vehicle crossing speed bumps of fixed dimensions. According to [16], speed bumps in Vietnam include several types, such as clustered speed bumps and rumble strips. This study focuses on vehicles navigating on rumble strips spaced 3-5 m apart, with a minimum deceleration distance covering 10 ridges. A speed reduction from 30-40 km/h to 10-15 km/h is proposed, with the selected vehicle speed for this analysis being set at 15 km/h (4.17 m/s). The rumble strip parameters include a width of 200 mm, a thickness of 4 mm, and a spacing of 3 m between the bumps. The MATLAB Simulink software is used to calculate the force applied to the vehicle’s body as it traverses the rumble strips, as exhibited in Figure 4.

The results indicate that the excitation force exerted by the speed bumps reaches a peak of approximately 275 N at the front axle and 610 N at the rear axle. These values are utilized to define the amplitude of the excitation force for the sound pressure analysis. The forces are applied directly above each wheel, as shown in Figure 5, with measurement nodes being positioned at the driver’s ear (ID 209322) and passenger ear positions (IDs 204269, 198303, and 238706).

Figure 6 depicts the SPL at the driver's ear position across the frequency range of 0 to 200 Hz. The results indicate a relatively large SPL range, varying from 67.08 dB to 166.92 dB. The peak values along the pressure curve range from 126 dB to 166 dB, exceeding the human hearing threshold of 120 dB.

Figure 7 highlights the frequencies producing an SPL exceeding 120 dB. The analysis reveals that, out of the 200 frequencies examined, 75 surpass this threshold. Notably, 24 of the 33 frequencies generating high sound pressure are concentrated within the 121 Hz to 154 Hz range. Furthermore,

as shown in Table V, a resonance phenomenon occurs at 176 Hz at the driver's position. This occurs when the excitation frequency closely matches the natural frequencies of the air mass (176.46 Hz) and the vehicle body (176.44 Hz), leading to a maximum SPL of 166.92 dB.

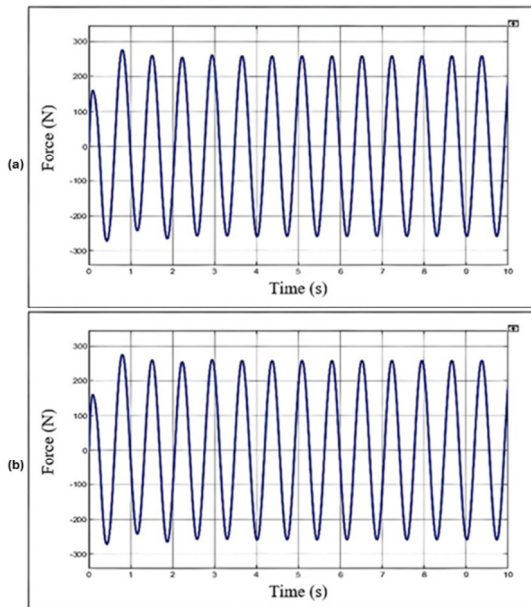


Fig. 4. Force applied to: (a) the front axle and (b) rear axle.

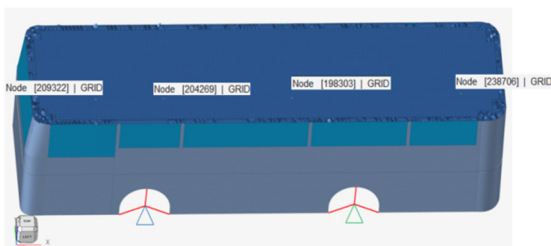


Fig. 5. Placement of the measurement nodes corresponding to the driver and the passenger positions.

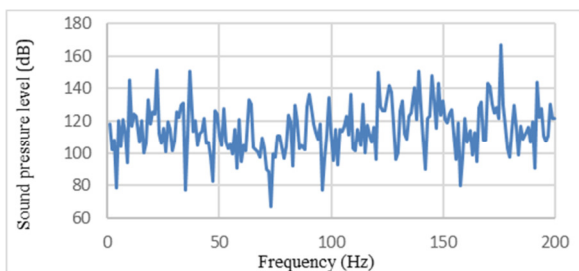


Fig. 6. SPL at the driver's ear position ID 209322.

Figure 8 presents the SPL at the three passenger seating positions across the frequency range of 0 to 200 Hz. The graph indicates that, overall, the SPL distribution at all three positions remains relatively consistent within this range, fluctuating primarily between 100 and 130 dB. However, the highest SPL within this frequency range exhibits a notable discrepancy among the three seating positions.

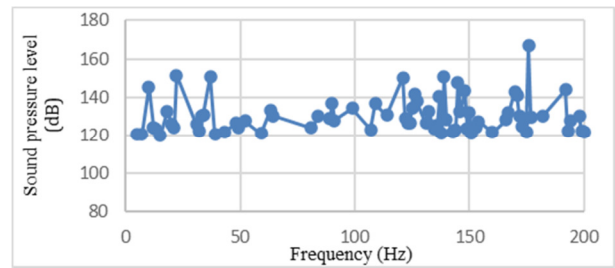


Fig. 7. Frequencies that produce an SPL greater than 120 dB.

TABLE V. COMPARISON TABLE OF SOUND RESONANCE EVALUATION AT DRIVER'S POSITION

Frequencies at the peaks of the sound pressure curve (Hz)	The natural frequency of the air mass (Hz)	The natural frequency of the car body shells (Hz)
81	82.14	82.13
145	144.57	144.59
<b>176</b>	<b>176.46</b>	<b>176.44</b>
192	190.01	190.004

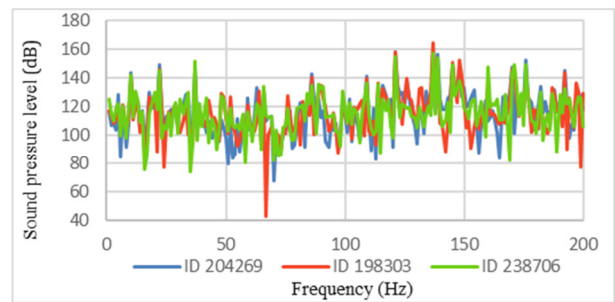


Fig. 8. SPL at three passenger seating positions across the frequency range of 0 to 200 Hz.

Table VI shows the maximum SPL value generated at three passenger seating positions. It can be observed that at a frequency of 137 Hz, all three passenger seat positions recorded maximum SPLs. The middle row seat (ID 198303) reached the highest SPL of 164.12 dB, while the rear seat (ID 238706) produced the lowest SPL among the three examined positions.

TABLE VI. MAXIMUM SPL VALUE GENERATED AT THREE PASSENGER SEATING POSITIONS

Seat position	Maximum SPL (dB)	Frequency (Hz)
ID 204269	161.13	137
ID 198303	164.12	137
ID 238706	157.34	137

### E. Noise Analysis Problem at the Driver's Position after the Car Moves on Uneven Road Surface

As the vehicle moves over an uneven road surface, it encounters various road profiles, causing the excitation force transmitted from the road to the vehicle body to fluctuate over time. As a result, the SPL inside the cabin varies during the vehicle's operation. This study focuses on the CD road type (medium road) according to the ISO 8608:1995 standard [19]. The MATLAB Simulink software is employed to simulate the excitation amplitude from the CD road and the excitation

force applied on the vehicle's two axles over a 25-second period, as can be seen in Figures 9 and 10.

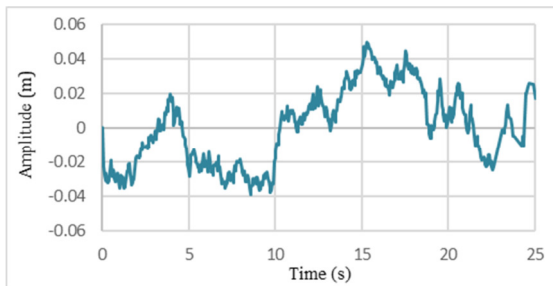


Fig. 9. CD pavement amplitude over a period of 25 s.

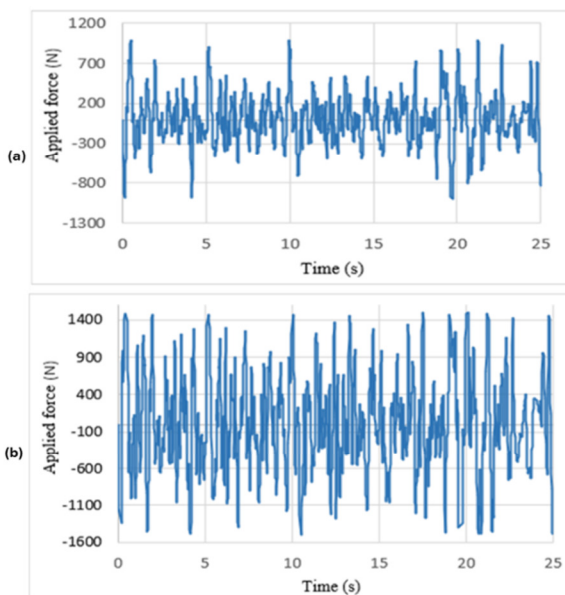


Fig. 10. Stimulating force from the road surface applied (a) to the front axle and (b) to the rear axle.

Since the forces are calculated using the 1/2 suspension system simulation equation, this study assumes that both wheels on the same axle receive excitation of the same magnitude and at the same time. The excitation forces from the road acting on the front and rear axles will be applied sequentially to the two front wheels and the two rear wheels. The applied forces are positioned directly above each wheel, as illustrated in Figure 5.

Hearing is believed to be affected by the changes in atmospheric pressure, either during or immediately after these changes have occurred [20]. The noise generated inside the cabin causes the surrounding air to compress and expand, creating a pressure differential relative to the atmospheric pressure. A sudden or continuous pressure differential of 3 to 5 psi can be harmful to hearing [21]. Figure 11 portrays the sound pressure obtained at the driver's position. The results indicate that the noise within the cabin creates the largest pressure differential of approximately 1653.8 Pa (0.24 psi), at 5.78 sec, which is significantly lower than the threshold that could potentially harm the human hearing.

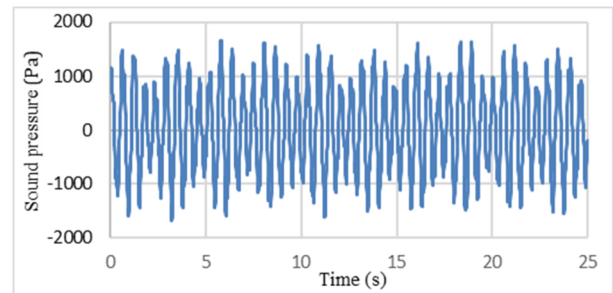


Fig. 11. Sound pressure obtained from driver's position for 25 s.

To visually assess the cabin noise, it is crucial to analyze SPLs (dB), which reflect the human hearing perception. The results derived from Figure 12 reveal that during 25 seconds of driving on an uneven road, the driver experiences sound levels ranging from 82 dB to approximately 155 dB. Specifically, the continuous SPL for the driver fluctuates between 130 dB and 155 dB, as indicated by the bold line on the graph. This level significantly exceeds the average hearing threshold of 120 dB, which can be attributed to the simulation model's exclusion of various details, such as the suspension system, plastic panels, soundproofing foam, and other interior components.

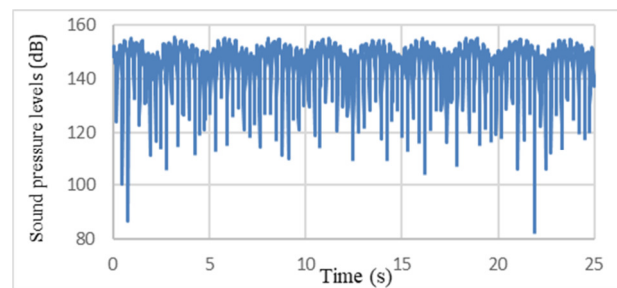


Fig. 12. SPL at the driver's position in 25 s.

#### IV. CONCLUSIONS

This study provides valuable insights into the impact of vehicle body vibrations and noise on cabin acoustics, particularly focusing on the Thaco Garden TB79S bus. Through simulations of two distinct scenarios- traversing speed bumps and driving on a CD road surface- the study identifies significant Sound Pressure Levels (SPLs), especially at the driver's ear, where resonance phenomena at 176 Hz led to peak SPLs of 166.92 dB. The analysis of the sound pressure fluctuations during travel on uneven surfaces revealed a maximum pressure differential of 0.24 psi, which, although not harmful to the hearing, resulted in high SPLs fluctuating between 130 dB and 155 dB. These levels far exceed typical cabin noise levels and the threshold for human hearing.

The results highlight the limitations of the model used in the current study, which excludes the key soundproofing elements present in real vehicles, such as insulation materials and interior components. This omission explains the observed higher-than-expected SPLs. Future research should focus on developing more comprehensive models that incorporate these components, allowing for a more accurate assessment of noise and vibration reduction strategies. Additionally, real-world data

collected from road tests, along with advanced sensors, will enhance individuals' understanding of how different driving conditions and vehicle components contribute to noise and vibration, providing further insights for improving vehicle comfort and safety.

#### REFERENCES

- [1] P. T. Long and L. D. Hoa, "Evaluation of aerodynamic noises for passenger cars using numerical method," *Tạp chí Khoa học và Công nghệ - Đại học Đà Nẵng*, vol. 18, no. 8, pp. 1–6, Aug. 2020, <https://jst-ud.vn/jst-ud/article/view/3315>.
- [2] D. H. Vu, T. T. Phong, N. T. Thuy, and L. K. Oanh, "Effect of Internal Combustion Engine Vibrations on Vehicle Ride Comfort," *International Journal of Advances in Engineering and Management (IJAEM)*, vol. 4, no. 6, pp. 1047–2052, Jun. 2022, <https://doi.org/10.35629/5252-040610471051>.
- [3] N. P. T. Luu, "A study on vibration and noise of differential by using comsol multiphysics simulation," *Journal of Technical Education Science*, vol. 16, no. 3, pp. 99–105, Jun. 2021, <https://doi.org/10.54644/jte.64.2021.99>.
- [4] N. Q. Cường, N. V. Bang, and N. T. Lập, "PHÂN TÍCH RUNG ĐỘNG CỦA KẾT CẤU KHUNG VỎ Ô TÔ CON DƯỚI SỰ KÍCH THÍCH TỪ ĐỘNG CƠ," *Tạp chí Khoa học & Công nghệ*, vol. 56, no. 3, pp. 89–93, Jun. 2020.
- [5] T. M. Nguyen, L. D. Vu, and Q. Nguyen, "Evaluation Motion Comfort of Sleeper Coach, the Type of Vehicle Is Manufactured and Assembled at Vietnam, Effect of Random Road Profile Based on Standard ISO 8608," in *Advances in Engineering Research and Application*, Cham, 2020, pp. 303–309, [https://doi.org/10.1007/978-3-030-37497-6\\_35](https://doi.org/10.1007/978-3-030-37497-6_35).
- [6] S. Kim and M. E. Altinsoy, "Active control of road noise considering the vibro-acoustic transfer path of a passenger car," *Applied Acoustics*, vol. 192, Apr. 2022, Art. no. 108741, <https://doi.org/10.1016/j.apacoust.2022.108741>.
- [7] G. Przydatek, A. Ryniewicz, O. Irimia, C. Tomozei, E. Mosnegutu, and M. Bodziony, "Analysis of Noise Levels in Typical Passenger Cars," *Sustainability*, vol. 15, no. 10, Jan. 2023, Art. no. 7910, <https://doi.org/10.3390/su15107910>.
- [8] M. Misol, S. Algermissen, and H. P. Monner, "Experimental investigation of different active noise control concepts applied to a passenger car equipped with an active windshield," *Journal of Sound and Vibration*, vol. 331, no. 10, pp. 2209–2219, May 2012, <https://doi.org/10.1016/j.jsv.2012.01.001>.
- [9] J. Gomez *et al.*, "Analysis of acoustic characteristics of a car cabin using computer-aided engineering," *Applied Mechanics and Materials*, vol. 268–270, pp. 883–889, 2013, <https://doi.org/10.4028/www.scientific.net/AMM.268-270.883>.
- [10] M. R. Forouzan and R. Hoseini, "Dynamic analysis of a modified truck chassis," *Int J Advanced Design and Manufacturing Technology*, vol. 3, no. 4, Sept. 2010.
- [11] J. Marzbanrad and M. Alahyari Beyg, "Vehicle Cabin Noise Simulation due to High-frequencies Stimulation," *Automotive Science and Engineering*, vol. 2, no. 2, pp. 117–123, Apr. 2012.
- [12] S. Hatture, R. Patil, and Dr. Jeyanthi S, "Analysis of Sound Pressure Level Inside Car Cabin," Jul. 2018.
- [13] J.-F. Durand, C. Soize, and L. Gagliardini, "Structural-acoustic modeling of automotive vehicles in presence of uncertainties and experimental identification and validation," *The Journal of the Acoustical Society of America*, vol. 124, no. 3, pp. 1513–1525, 2008.
- [14] S. A. Patil and R. R. Arakerimath, "Parametric Optimization of Biodiesel Fuelled Engine Noise using the Taguchi Method," *Engineering, Technology & Applied Science Research*, vol. 10, no. 4, pp. 6076–6079, Aug. 2020, <https://doi.org/10.48084/etasr.3595>.
- [15] S. Mogal, A. Kapse, V. Shewale, and P. Shete, "An Experimental Investigation of the Effects of Diesel-Ethanol Blends on the Noise and Vibrations of a Diesel Engine," *Engineering, Technology & Applied Science Research*, vol. 13, no. 3, pp. 10875–10881, Jun. 2023, <https://doi.org/10.48084/etasr.5867>.
- [16] *Speed Humps, Speed Humps on Roads - Design Requirements*, TCCS 34: 2020/TCDBVN, Vietnam Road Administration, Vietnam, Dec. 2020, <https://thuvienphapluat.vn/van-ban/Giao-thong-Van-tai/Quyet-dinh-6500-QD-TCDBVN-2020-cong-bo-Tieu-chuan-co-so-Go-giam-toc-go-giam-toc-tren-duong-bo-495053.aspx>.
- [17] S. Patil, G. U. Raju, and C. Chavan, "NVH Analysis of Car Cabin Compartment," *International Journal of Scientific Development and Research (IJS DR)*, vol. 3, no. 7, pp. 317–324, Jul. 2018.
- [18] S. Rao and A. Bhattu, "Dynamic Analysis and Design Modification of a Ladder Chassis Frame Using Finite Element Method," *Amity Journal of Computational Sciences (AJCS)*, vol. 1, no. 2, pp. 16–22, 2017.
- [19] *Mechanical Vibration-Road Surface Profiles-Reporting of Measured Data*, ISO 8608:1995, Sept. 1995.
- [20] M. Kitahara, H. Ozawa, A. Kodama, H. Izukura, S. Inoue, and K. Uchida, "Effect of Atmospheric Pressure on Hearing in Normal Subjects," *Acta Oto-Laryngologica*, vol. 114, no. sup510, pp. 87–91, Jan. 1994, <https://doi.org/10.3109/00016489409127310>.
- [21] W. J. Staab, "Risk Factors Associated With Environmental Pressure Changes on Tympanic Membrane Rupture and Ear Damage," *Canadian Audiologist*, vol. 8, no. 5, Aug. 2021.